Leveraging Fracture Toughness and Corrosion Resistance in the Development of Advanced High-Strength Steels for Automotive Chassis and Frame Applications

Arjan Rijkenberg, Toni Chezan, Arnoud de Vooys
Tata Steel, PO Box 10.000, 1970 CA IJmuiden, The Netherlands

Abstract

HSLA and CP for automotive chassis and frame must provide excellent HEC and fracture toughness. However, this poses challenges as HEC and fracture toughness are not always mutually consistent due to different microstructural dependencies and the influence of secondary cold work embrittlement. This study shows that CP provides an optimal balance between HEC and fracture toughness compared to HSLA. However, the need for hardenability for bainitic CP also draws attention to another crucial feature of exposed automotive parts: corrosion resistance. SAE J2334 tests were done on HR660Y760T-CP with various Mn, Cr, and Mo contents, revealing essential differences in corrosion resistance. Insights into the relationship between HEC and toughness and the role of alloy composition on corrosion resistance were leveraged in the development of a new bainitic HR660Y760T-CP grade.

1. Introduction

Efforts to save vehicle weight to reduce emissions and increase driving range extend to automotive chassis and frame applications. Common steels for such applications are hot-rolled ferritic High-Strength Low-Alloy (HSLA) and bainitic Complex Phase (CP) steels. In addition to high strength to save weight via down gauging, these steels must provide optimal global and local formability or elongation and hole-expansion (HE) capacity (HEC) for component geometry optimisation [1].

From a materials perspective, high HEC can be achieved via two approaches highlighted in Figure 1a. The first approach is to break free from the constraint between HEC and elongation [2]. This is done by producing essentially single-phase ferritic or bainitic steels that do not rely for strength on µm-sized second-phase constituents, which promote damage and voids upon shearing [3-8], but instead derive strength from nm-sized precipitates that do not promote substantial void formation upon shearing [2]. These steels offer an exceptional balance between HEC and elongation with HEC largely controlled by plasticity (r-value, planar anisotropy) [3,9,10]. The second approach is to produce steels that derive strength from transformation and for which strain incompatibility between matrix and second-phase are reduced [3-8] via transformation strengthening and optionally precipitation strengthening of the matrix. This approach results in a trade-off between HEC and elongation.

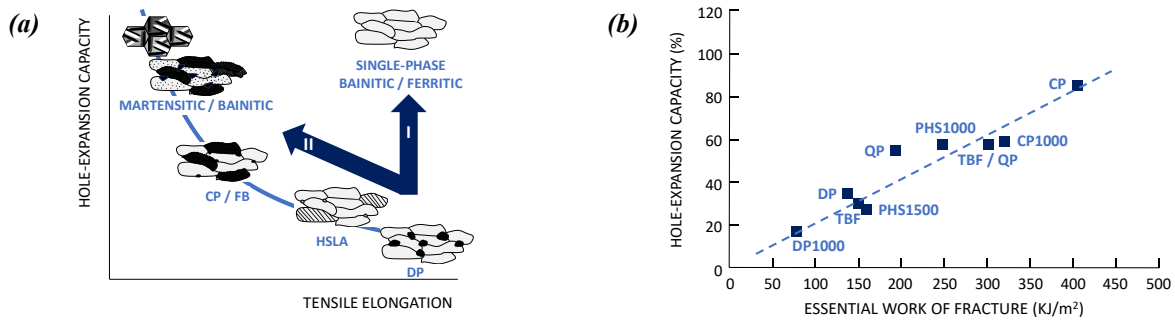

Figure 1. The relationship between (a) HEC and elongation [2] and (b) HEC and essential work of fracture from [11]

Several studies [11,12] have found a linear correlation between HEC and fracture toughness (Figure 1b), which suggests that increased HEC and thus increased fracture toughness provides robust manufacturing. However, stress-strain conditions imposed on edges during manufacturing are often very different and more complex than those in the HE test. The HE test excludes the effect of alternating stresses due to successive forming steps and springback, which can activate secondary cold work embrittlement (CWE) [13] that reduces fracture toughness and leads to issues with unpredicted edge cracks, even though the steel offers high HEC.

In this context, Tata Steel has adopted a deep-draw cup (DDC) test [14] to assess a measure for edge-crack susceptibility and fracture toughness. This test screens steels on susceptibility to secondary cold work embrittlement [15,16] and fracture toughness. In the first part of this study, the DDC test was used for a series of high-strength hot-rolled ferritic HSLA and bainitic CP steels. The outcome was used further to study the relationship between HEC and toughness and how microstructural features, like grain size, second-phase fraction, and texture play a role. The results show the relevance of microstructural control for an optimal balance between HEC and toughness and that bainitic CP steels provides a superior balance.

These bainitic steels are at least partly achieved via suitable alloying for sufficient hardenability, which is commonly done with manganese, (Mn), chromium (Cr), and molybdenum (Mo). However, these elements not only indirectly influence formability and ductility, but also impact another, unrelated characteristic: corrosion resistance. This aspect is important for exposed automotive components in chassis and frame, as corrosion resistance affects in-service lifetime, structural integrity, and safety. In the second part of this study, the influence of Mn, Cr, and Mo on the corrosion resistance of HR660Y760T-CP steels is investigated. This is done with the SAE J2334 test as this test correlates well with the degradation mechanisms that occur in real-life for vehicles [17].

This study concludes with the introduction of a new bainitic MP800 steel grade (HR660Y760T-CP) for automotive chassis and frame applications, which has been developed using all the knowledge developed in this paper to achieve high HEC, adequate toughness and corrosion resistance.

2. Laboratory Study on Hole-Expansion Capacity and Fracture Toughness

A laboratory study was conducted to study the ability of the DDC test to screen steels for crack susceptibility and fracture toughness and to learn how the results of the DDC test compare to those of the HE test to understand the relationship between fracture toughness and HEC. As part of this study, a series of hot-rolled ferritic HSLA and bainitic CP steels were produced with different alloys and process settings. The first two Sections present the experimental design (Section 2A) and details of the DDC test (Section 2B). In Section 2C the results are presented. In Section 2D, a discussion on the relationship between fracture toughness and impact toughness for the laboratory steels is presented, followed by Section 2E with the fracture toughness of several industrial steels. Sections 2D and 2E both illustrate the ability of the DDC test to distinguish steels with diverse microstructures on crack sensitivity and fracture toughness. Finally, Sections 2F and 2G focus on the relationship between HEC and fracture toughness for the laboratory steels and several industrial steels.

2A. Experimental

As part of the laboratory study, ten alloys were vacuum melted and ingot cast. The compositions are shown in Table 1. The top five alloys were used to produce precipitation-strengthened ferritic (F) or HSLA-type steels and are labelled by micro-alloy (MA) and carbon (C) content. As MA agents, niobium (Nb), titanium (Ti), and vanadium (V) were used. These three elements each influence the recrystallisation of austenite during hot rolling to a varying degree (Nb > Ti > V) and hence influence the non-recrystallisation temperature (T_{nr}), r-values, and planar anisotropy of the steel [18,19]. For the F-V, F-NbV, F-TiV, and F-Ti alloys, the ratio between C content and that of the sum of precipitating elements Nb, Ti, V, and molybdenum (Mo) was chosen such that carbon levels were nearly (sub)stochiometric, thus suppressing the formation of carbon-rich second-phase constituents other than nm-sized carbide and carbonitride precipitates. For the F-CV alloy, the C and V contents were chosen to achieve carbon overstochiometry to promote carbon-rich second-phase constituents in addition to fine carbide and carbonitride precipitates. The bottom five alloys were used to produce TiC-enforced bainitic (B) or CP-type steels and are labelled by C, boron (B), and Ti content. For the B-LCB alloy, a low C content was chosen to promote an essentially TiC-strengthened single-phase bainitic microstructure and – next to Mo present in all B alloys – boron was added to ensure sufficient hardenability. For B-MC, B-HC, and B-EHC, the C content was varied to promote differences in carbon-rich second-phase fractions in the bainitic microstructure (martensite and cementite). The B-HCTi- alloy was introduced to study the effect of reduced Ti on T_{nr}, r-value, and planar anisotropy.

The ingots were forged from 105 to 35 mm thickness after 1240 °C reheating and cooled to ambient temperature before being sawn in smaller blocks of 75 x 105 mm. These blocks were rolled in a 4-pass rolling schedule to 3.5 mm in a single-stand mill after reheating to 1240 °C for 40 minutes. Finish-rolling temperatures (FRT) of 980 and 890 °C were used to study the effect of finish rolling on planar anisotropy and grain size. After hot rolling, the plates of 750 x 105 x 3.5 mm were directly transferred to a run-out-table (ROT) and cooled with a mixture of water and pressurized air before being placed in a furnace to replicate coil cooling. For the ferritic steels, the exit ROT and furnace temperatures were 580 and 630 °C. For the bainitic steels, the exit ROT and furnace temperatures were 400 and 450 °C. Variation in coiling temperatures (CT) was introduced to study the effect of a change in microstructure (e.g., grain size, second-phase constituents) on HEC and toughness. The ROT cooling rate in all cases was circa 50 °C/s and all plates were shot-blasted to remove oxides from the hot-rolling process.

Table 1. Compositions (in wt-%) of the hot-rolled ferritic (F) and bainitic (B) steels of the laboratory study

Alloy	Type	C	Mn	Si	Al	Nb	Ti	V	Mo	B	N
F-CV	HSLA	0.20	1.60	0.40	0.065	-	-	0.15	0.30	-	0.001
F-V	HSLA	0.10	1.60	0.40	0.065	-	-	0.30	0.30	-	0.001
F-NbV	HSLA	0.10	1.60	0.40	0.065	0.56	-	0.30	0.30	-	0.001
F-TiV	HSLA	0.10	1.60	0.40	0.065	-	0.10	0.15	0.30	-	0.001
F-Ti	HSLA	0.10	1.60	0.40	0.065	-	0.20	-	0.30	-	0.001
B-LCB	CP	0.06	1.90	0.40	0.065	-	0.13	-	0.25	0.002	0.001
B-MC	CP	0.12	1.90	0.40	0.065	-	0.13	-	0.25	-	0.001
B-HC	CP	0.16	1.90	0.40	0.065	-	0.13	-	0.25	-	0.001
B-HCTi-	CP	0.16	1.90	0.40	0.065	-	0.05	-	0.25	-	0.001
B-EHC	CP	0.24	1.90	0.40	0.065	-	0.13	-	0.25	-	0.001

For each steel variant, three plates were selected for testing and analysis. Each of these three plates was used for A50 tensile tests in longitudinal direction (L) according to ISO 6892 and the rest of the plate was used for: (1) HE tests, (2) Charpy V-notch (CVN) impact tests, and (3) DDC tests. Transverse A50 samples were not possible due to too small strip width. The HE tests were performed according to ISO 16630 in triplicate with 90 x 90 mm blanks punched with a flat punch and 12% clearance. The HE test was performed burr upwards with a conical punch (60° apex angle). The CVN tests were done in triplicate at test temperatures of -60, -40, -20, 0, and +20 °C to determine the absorbed energy (KV) and the transition temperature (TT). The samples measured 55 x 10 mm with the thickness identical to the as-rolled thickness in order to probe the material over the full thickness. The V-notch (ISO 148-1) was oriented parallel to rolling direction, yielding a main RD-ND fracture plane. The DDC test to assess crack susceptibility and the work of fracture of steels was done as described in Section 2B. For each steel variant, three cups were tested with the DDC test. However, experimental challenges occasionally led to test failure due to excessive or irregular fracture during deep drawing.

Microstructural analysis was done with Scanning Electron Microscopy (SEM) and Electron Backscatter Diffraction (EBSD) on longitudinal cross sections at ¼ thickness. Secondary electron (SE) imaging was done on polished and mildly etched (0.5% Nital for 2 seconds) cross sections. The SEM used was a Zeiss Ultra 55 with a Field Emission Gun and EDAX PEGASUS XM 4 HIKARI EBSD system. Texture analysis was done with X-Ray Diffraction (XRD) on a fully automated Bruker D8 diffractometer (CoKα-radiation and primary graphite monochromator) equipped with a 2D area detector (GADDS). Details on EBSD and XRD settings as well as procedures for data analyses are given in Reference [20].

2B. Deep-Draw Cup (DDC) Test Procedure

A deep-draw cup (DDC) test [14] was used to assess the crack susceptibility and the work of fracture of steels under conditions relevant to component manufacturing. The test consists of two parts: (1) deep-drawing to assess crack susceptibility due to secondary cold work embrittlement [15,16] and (2) cup-compression to assess the energy required for (further) crack growth.

Details of the deep-drawing stage are illustrated in Figure 2. The blank size is 90 x 90 mm with each of the four corners cut 10 mm diagonally for geometric limitations of the experimental setup. A punch with a diameter of 50 mm and a radius of 7 mm is used for deep drawing. The die has an inner diameter of 62 mm and a radius of 8 mm. The inner die is chosen sufficiently large to allow free movement of the cup edge. The distance between punch and die wall is 6 mm and the blank holder force is 50 kN.

During the deep-drawing stage, the four locations indicated by circles in Figure 2c are compressed, resulting locally in surface roughening of the sheared edges, as illustrated in Figure 2d. At the end of the test and upon release of the blank holder force, the four compressed regions are subject to reverse loading due to springback as the formed cylindrical cup starts to lose contact with the blank holder. This reverse loading can lead to the nucleation and growth of cracks in the compressed regions of the cup due to secondary cold work embrittlement. Cracks may be present through the full thickness and visible on the in- and outside of the cup wall, or may be present only on one side. The length of each crack visible on the in- and outside of the compressed edges is measured using a magnifying glass with a scale grid, summed, averaged, and reported as the total crack length (TCL) in mm.

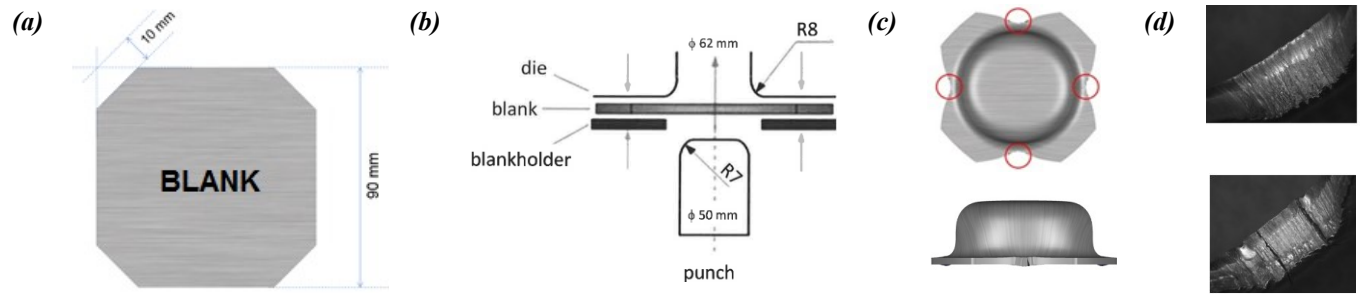

Figure 2. Images illustrating the deep-drawing stage of the DDC test: (a) blank shape and size, (b) schematic experimental setup, (c) deep-drawn cup with compressed regions encircled, and (d) images of compressed edges without and with cracks

In the second part of the DDC test, the energy required for crack growth or the work of fracture is determined by compressing the deep-drawn cups between a cone and a flat tool in a conventional tensile testing machine (Figure 3a), where the normal of the flat plane and the axis of the cone are parallel. The cone has an angle of 90° and touches the inner wall of the cup. As the flat tool moves towards the cone, it exerts a normal force on the flat bottom of the cup. The cone exerts forces on the wall of the cup resulting in crack growth from the four regions of the compressed edges of the cup. The normal force on the flat plate is recorded as a function of the plate displacement. The test stops a few mm before the flat bottom of the cup touches the top of the cone. For the selected geometry, a maximum displacement up to 12 mm can be recorded. The area under the force-displacement curve is taken as an estimate of the steel's resistance to crack initiation and propagation and is considered a measure of the fracture toughness. For this study, the area up to a displacement of 10 mm was calculated and defined as the work of fracture (WOF). To take into account the effect of thickness, the WOF value (in J) is divided by the thickness of the steel sheet (J/mm) to ensure a fair comparison between steels with different thickness. Figure 3b shows examples of a deep-drawn and a compressed cup. Examples of force-displacement curves for predominantly ductile and brittle fracture are shown in Figure 3c. The latter curve with intermediate abrupt load drops as a result of brittle crack propagation shows evidence of alternating ductile and brittle fracture behaviour.

Figure 3. Images of (a) the experimental setup for the cup-opening stage of the DDC test, (b) the effect on deep-drawn cups, and (c) examples of force-displacement curves for steels with ductile and alternating ductile-brittle fracture behaviour

2C. Results

The A50 tensile properties in longitudinal direction (L) and HEC (λ) values of the ferritic and bainitic steels are given in Tables 2 and 3. Also shown here are the TCL and WOF values from DDC testing, the KV_{+20} and KV_{-60} values from CVN testing, and the TT values derived from fitting the CVN impact toughness transition curves with the hyperbolic tangent equation [21]

$$KV = \left(\frac{USE+LSE}{2}\right) + \left(\frac{USE-LSE}{2}\right)\tanh\left[\frac{T-TT}{C}\right] \quad [1]$$

with USE and LSE corresponding with the upper shelf and lower shelf energy, T being the test temperature (in °C), and C the half-width of the transition region. The USE and LSE values for all steels were 135 and 7 J/cm^2.

Table 2. Tensile properties (L), HEC, DDC, and CVN data for the laboratory hot-rolled ferritic steels

Steel	Process	Rp (MPa)	Rm (MPa)	A50 (%)	r_0 (-)	HEC (%)	TCL (mm)	WOF (J/mm)	KV_{+20} (J/cm^2)	KV_{-60} (J/cm^2)	TT (°C)
F-CV	**980-630**	606	759	16.2	0.82	62	26.5	40	66	33	+23
	980-580	631	820	15.0	0.83	43	11.7	34	38	12	+60
	890-630	620	757	17.7	0.78	50	54.2	61	80	32	+1
	890-580	730	889	15.0	0.76	31	21.9	50	53	17	+36
F-V	**980-630**	738	839	15.8	0.81	137	43.5	24	91	15	-18
	980-580	683	878	15.0	0.80	86	55.1	23	76	9	+13
	890-630	787	861	16.2	0.75	112	26.0	44	108	13	-16
	890-580	833	937	14.7	0.72	77	42.3	31	88	13	+4
F-NbV	**980-630**	717	846	16.7	0.73	47	43.9	47	100	46	-33
	980-580	788	905	14.7	0.71	95	27.9	49	105	28	-23
	890-630	699	822	17.0	0.71	44	33.6	71	107	72	-77
	890-580	773	883	15.8	0.68	51	21.8	88	116	69	-75
F-TiV	**980-630**	916	986	15.5	0.73	65	104.8	21	27	9	+74
	980-580	937	1032	13.2	0.80	27	66.3	22	19	8	+78
	890-630	936	998	16.8	0.75	57	36.5	35	40	13	+56
	890-580	1004	1056	15.0	0.66	49	50.2	25	46	11	+37
F-Ti	**980-630**	895	968	16.3	0.76	30	71.0	20	36	9	+48
	980-580	969	1032	15.0	0.76	51	75.0	22	29	9	+59
	890-630	915	974	17.1	0.65	32	32.6	41	64	21	+21
	890-580	958	1009	15.9	0.68	28	49.0	35	78	23	+2

Table 3. Tensile properties (L), HEC, DDC, and CVN data for the laboratory hot-rolled bainitic steels

Steel	Process	Rp (MPa)	Rm (MPa)	A50 (%)	r_0 (-)	HEC (%)	TCL (mm)	WOF (J/mm)	KV_{+20} (J/cm^2)	KV_{-60} (J/cm^2)	TT (°C)
B-LCB	**980-450**	852	953	11.0	0.86	80	1.8	124	133	60	-54
	980-400	877	987	9.7	0.86	93	0.9	123	123	83	-75
	890-450	828	925	10.8	0.73	80	1.1	159	144	86	-86
	890-400	878	975	8.1	0.77	57	2.1	162	95	73	-69
B-MC	**980-450**	778	874	12.3	0.71	86	2.1	132	131	63	-69
	980-400	789	915	9.2	0.72	70	1.2	143	129	65	-63
	890-450	810	881	9.6	0.70	76	0.0	162	128	87	-89
	890-400	781	888	11.0	0.68	70	0.0	179	133	80	-86
B-HC	**980-450**	828	922	10.7	0.69	71	0.9	134	105	53	-48
	980-400	911	1029	7.2	0.69	51	8.4	119	97	31	-20
	890-450	842	917	12.2	0.63	57	1.7	162	119	72	-72
	890-400	821	932	9.9	0.62	63	0.0	164	103	62	-48
B-HCTi-	**980-450**	815	905	10.5	0.78	71	5.1	130	107	72	-74
	980-400	982	1090	7.8	0.75	70	1.1	137	96	42	-31
	890-450	775	867	12.0	0.67	72	0.0	169	105	73	-83
	890-400	876	979	8.7	0.84	83	2.3	153	123	81	-72
B-EHC	**980-450**	830	944	10.1	0.73	47	2.4	97	81	35	-4
	980-400	1087	1202	8.3	0.83	55	6.3	107	48	23	+53
	890-450	812	921	12.6	0.69	46	0.0	155	89	45	-20
	890-400	1004	1102	8.1	0.68	66	0.0	162	76	37	-2

The tensile strength of the ferritic steels ranges from 760 to 1060 MPa with A50 tensile elongations from 13 to almost 18%. The HEC shows a wide variation for the ferritic steels, ranging from 30% for some of the F-TiV and F-Ti steels to 137% for the F-V steel produced with high FRT and CT. The TCL of the ferritic steels is high with an average value of 45 ± 22 mm and individual values ranging from 10 to 105 mm. The WOF of the ferritic steels is low with an average value of 39 ± 18 J/mm and individual values ranging from 20 to 88 J/mm. The tensile strength of the bainitic steels ranges from 865 to 1200 MPa with A50 tensile elongations from 7 to almost 13 %, which is considerably lower than that of the ferritic steels. The HEC of the bainitic steels ranges from circa 45% for some of the B-EHC steels to 93% for the B-LCB steels with high FRT and low CT. The TCL of the bainitic steels is low with an average value of 1.9 ± 2.3 mm and individual values ranging from roughly 0 (free of cracks) to 9 mm. The WOF of the bainitic steels is high with an average value of 144 ± 22 J/mm and individual values ranging from 96 to 180 J/mm. A comparison between the TT for the ferritic and bainitic steels shows that generally the TT of the bainitic steels is considerably lower than that of the ferritic steels and that – in particular at -60 °C – their KV is generally substantially higher. This indicates a substantially higher impact toughness of the bainitic steels than that of the ferritic steels.

2D. Discussion – Fracture Toughness and Impact Toughness of the Laboratory Steels

Figure 4 shows the TCL of DDC tests for the ferritic and bainitic steels, highlighting a significant difference in crack susceptibility for both steels. The ferritic cups have an average TCL of 45 mm, while the average of the bainitic cups is much lower at an average of 1.9 mm, with several cups free of cracks. This difference is attributed to a combination of factors. Most important

are differences in the susceptibility to secondary cold work embrittlement and differences in the fracture toughness to resist further crack propagation from crack initiation sites caused by secondary cold work embrittlement. Another factor is the difference in the amount of springback during deep-drawing in the DDC test and the intensity of resulting tensile stresses on the compressed edges.

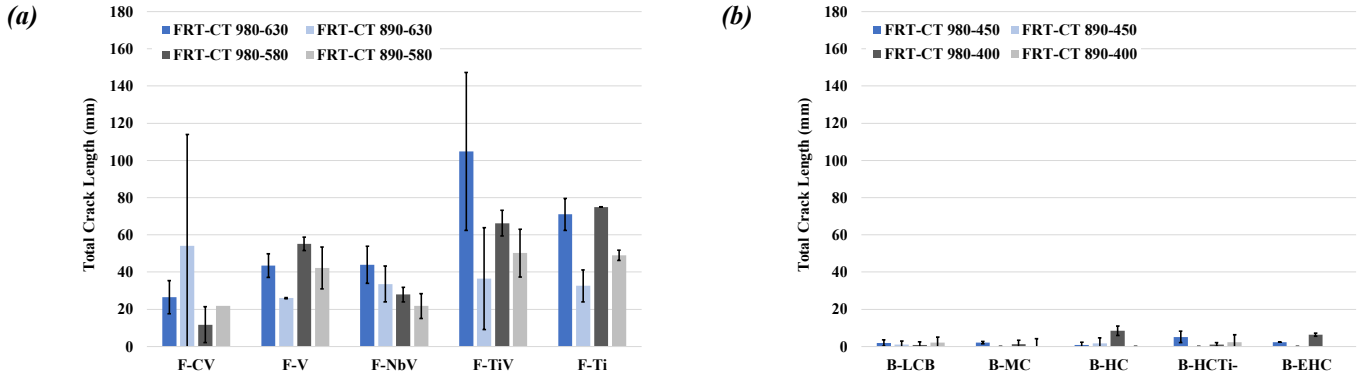

Figure 4. Total crack length of the laboratory hot-rolled (a) ferritic and (b) bainitic steels

Both springback and fracture toughness are related to yield strength. The amount of springback is related to the yield strength divided by the sheet thickness (Rp/t). A higher yield strength and lower thickness result in greater springback, which can increase secondary cold work embrittlement and thus increase crack susceptibility and TCL values. The relationship between yield strength and toughness is more complex because the different strengthening components that contribute to the yield strength have different influences on toughness. Only the Hall-Petch contribution (grain refinement) is beneficial. All other strengthening components, including solid-solution, precipitation, and dislocation strengthening reduce toughness. Therefore, increased yield strength that is not due to grain refinement inherently reduces toughness and yield increased crack susceptibility and increased TCL.

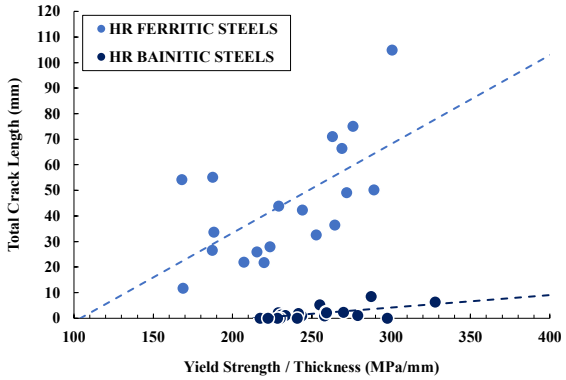

Figure 5. The total crack length versus the yield strength divided by the sheet thickness

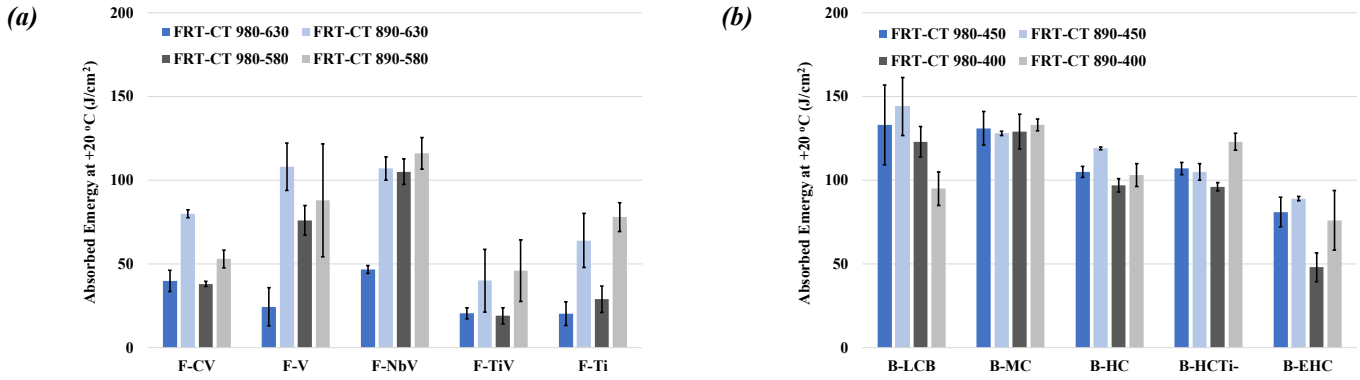

Figure 6. Absorbed energy from CVN testing at +20 °C for the laboratory hot-rolled (a) ferritic and (b) bainitic steels

Figure 5 shows a plot of TCL against Rp/t. For the ferritic steels, an increase in Rp/t (here controlled by an increase in Rp since the thickness of all steels is comparable) is accompanied by an increase in TCL. This fits with the expected influence of increased springback and reduced fracture toughness if the increase in Rp does not sufficiently arise from grain refinement. Similar data in Figure 5 for the bainitic steels also show this effect of Rp/t on TCL, albeit with a smaller gradient and overall effect than for the ferritic steels. Bainitic steels compared to ferritic steels with a similar Rp/t, and hence with a similar degree of springback, have substantially lower TCL values. This indicates that bainitic steels are less susceptible to crack initiation due to secondary cold work embrittlement than ferritic steels and that bainitic steels have significantly higher fracture toughness and hence better resistance to crack propagation. Studies on interstitial-free steels have shown that secondary cold work embrittlement and intergranular fracture can be suppressed by increasing grain boundary strength [13,15,16]. This in turn suggests a significant difference in grain boundary strength between ferritic and bainitic steels, although an investigation of this is beyond the scope of this study. As later confirmed in this study, the higher fracture toughness of bainitic steels is attributed to greater grain refinement.

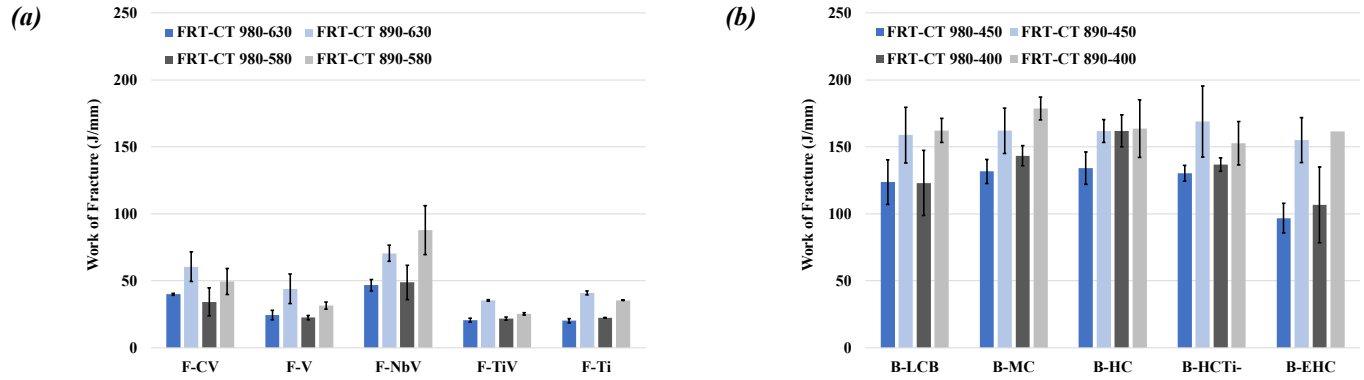

Figure 7. Work of fracture from DDC testing for the laboratory hot-rolled (a) ferritic and (b) bainitic steels

The higher toughness of the bainitic steels is confirmed by the data plotted in Figure 6 with the absorbed energy from CVN impact testing at +20 °C: the bainitic steels generally have a substantially higher toughness and hence a higher resistance to crack propagation. A similar conclusion, but now for data obtained with the DDC test can be drawn from the data plotted in Figure 7, showing the WOF data for the ferritic and bainitic steels as determined via cup-compression in the DDC test. Similar to the impact toughness data shown in Figure 6, here too a clear difference is seen between the ferritic and bainitic steels. The average WOF of the bainitic steels is relatively high at 144 J/mm, while that of the ferritic steels is much lower, averaging 39 J/mm.

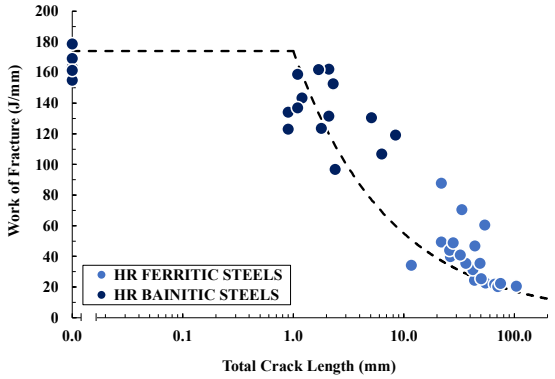

Figure 8. The work of fracture plotted against the total crack length

Unlike with CVN testing where all samples are in an identical initial sample condition with an identical blunt V-shaped notch, the initial sample state for the cup-compression stage in the DDC test is variable and highly dependent on the crack susceptibility of the sample during the initial cup deep-drawing stage of the DDC test. More and larger sharp cracks in the cups after deep drawing will promote increased local stress localisation during the subsequent cup-compression stage of the DDC test, facilitating crack propagation and reducing the energy required for crack propagation or the WOF. Figure 8 with the WOF plotted against the TCL for the ferritic and bainitic steels confirms the relationship between TCL and WOF. Beyond a TCL of circa 1 mm, the data plotted in Figure 8 follow Griffith's law [22] according to

$$\sigma_{fail} = K_{Ic} \frac{1}{\sqrt{\pi\, a}} \qquad [3]$$

with σ_{fail} as the stress at failure, K_{Ic} as the fracture toughness in mode I (opening mode with tensile stress normal to the crack plane) and a as the crack size. Beyond a TCL value of circa 1 mm the data from the DDC test follow

$$WOF = C \frac{1}{\sqrt{\pi\, TCL}} \qquad [4]$$

with constant C close to 308 J.mm$^{-0.5}$. Below a TCL of circa 1 mm, the WOF flattens out to a plateau around 175 J/mm.

Figure 9 shows that the WOF determined in the DDC test correlates with toughness. Figure 9a shows WOF versus absorbed energy (KV_{-60}) from CVN impact testing at -60 °C and Figure 9b shows WOF against the transition temperature (TT). Both graphs show the presence of two data populations, one for the ferritic and one, positioned significantly higher, for the bainitic steels. Within each population, WOF and KV_{-60} or WOF and TT - or fracture and impact toughness - show a linear relationship. This is expected since fracture and impact toughness are both controlled by crack propagation and thus determined by similar microstructural features of which grain size is a very important one, as will be shown later.

A comparison between the two data populations in Figures 9a and 9b shows that the bainitic steels generally have increased impact toughness with higher KV and lower TTs and that the WOF of the bainitic steels in all cases is substantially higher than that of the ferritic steels with equivalent KV and TT. This latter apparent discrepancy between impact and fracture toughness arises from an essential difference between the ferritic and bainitic steels in crack susceptibility during the deep-drawing stage of the DDC test due to different susceptibility to secondary cold work embrittlement. This in turn leads to different sample conditions prior to cup compression in the DDC test to determine the WOF. The crack-susceptible ferritic steels with high TCL values due to increased susceptibility to secondary cold work embrittlement have a multitude of cracks, while the more crack-resistant bainitic steels with significantly lower TCL values have no or only a few cracks. As Figure 8 and Equation 4 show, a higher TCL corresponds with a lower WOF, which is caused by the presence of sharp cracks that promote intense localised build-up of stresses at the crack tip during cup compression, reducing the energy required for crack propagation or WOF.

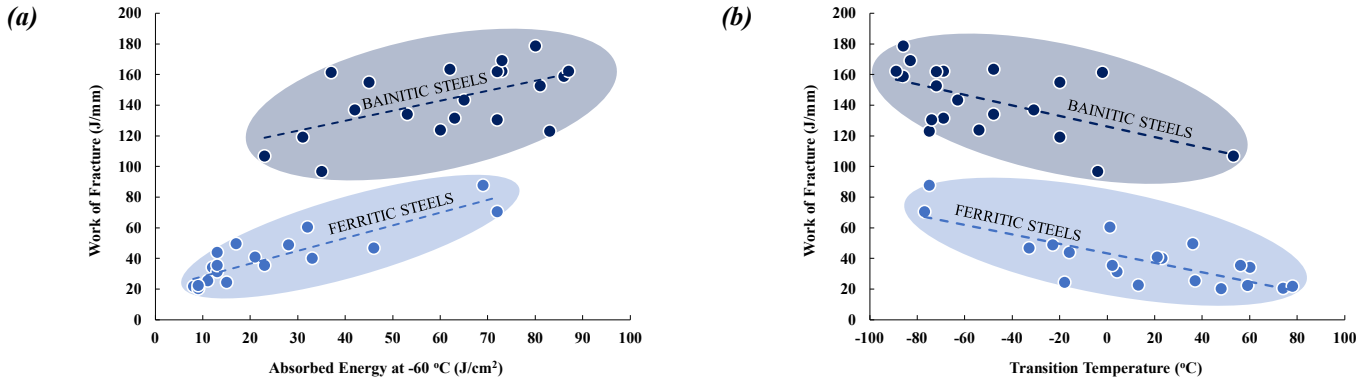

Figure 9. Work of fracture plotted against (a) the absorbed energy at -60 ºC and (b) the transition temperature

The ability of the DDC test to detect differences in crack susceptibility due to differences in secondary cold work embrittlement and to capture differences in the energy required for crack growth between different steel types under test conditions that represent component manufacturing conditions, makes the DDC test a valuable and even indispensable tool to supplement HE testing to assess the risk of edge cracking for different hot-rolled steel grades during automotive component manufacturing.

2E. Discussion – Fracture Toughness of Industrial Steels

The results of the laboratory study illustrate that the DDC test is an effective tool to screen steels for crack susceptibility due to differences in springback, secondary cold work embrittlement, and fracture toughness. It is considered a valuable testing procedure to include in the commercial development of steels to ensure that steels are fit for purpose for the production of automotive components. Figures 10 and 11 show the TCL and WOF values from DDC tests plotted against Rp/t for the laboratory hot-rolled ferritic and bainitic steels, but this time supplemented with comparable data for a number of industrial hot-rolled steels from regular production and works trials in an industrial hot-strip mill, including conventional ferritic HSLA (S500MC and S700MC labelled by Rp), high stretch-flangeability single-phase ferritic HSLA (S550SF, S700SF, and S850SF labelled by Rp), multi-phase AHSS (DP600, FB590, CP800 labelled by Rm), and martensitic UHSS (S960MC labelled by Rp) .

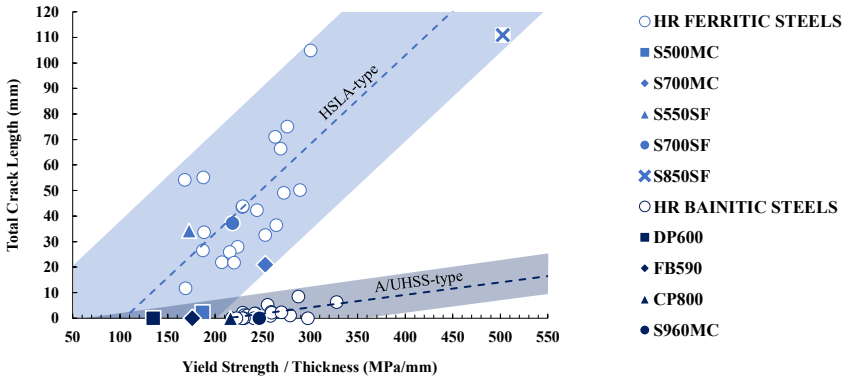

Figure 10. The total crack length versus Rp/t for a number of laboratory (open circles) and industrial hot-rolled grades

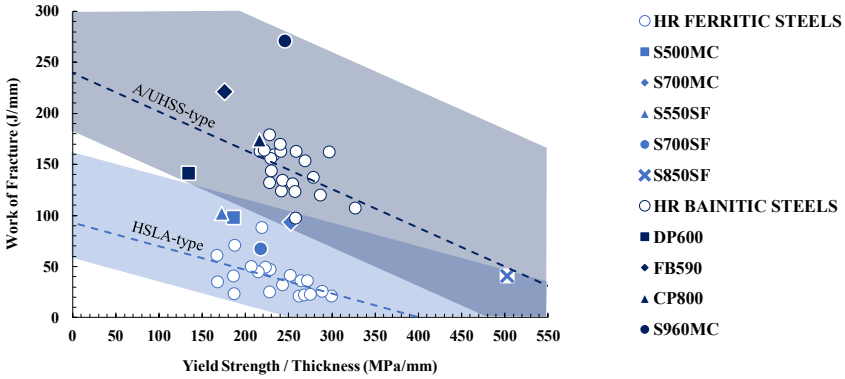

Figure 11. The work of fracture versus Rp/t for a number of laboratory (open circles) and industrial hot-rolled grades

The laboratory data plotted in Figures 10 and 11 show two regions, one for ferritic HSLA steels (light-blue region) and one for multi-phase, bainitic, and martensitic A/UHSS grades (dark-blue region). The conventional and stretch-flangeable ferritic HSLA steels show increased crack susceptibility compared to the A/UHSS grades with similar Rp/t values. Consequently, these latter steels show superior WOF in the DDC test compared to the conventional and stretch-flangeable ferritic HSLA steels as shown by the data plotted in Figure 11. This data from the DDC test is useful to assess the risk of edge cracking during component manufacturing.

2F. Discussion – Fracture Toughness and Hole-Expansion Capacity of Laboratory Steels

Several experimental studies have reported a linear relationship between fracture toughness and HEC [11,12]. In principle, this relationship is also expected because the energy required for crack growth which determines the steel's toughness, also plays an important role in the HE test as it involves crack propagation during hole expansion through the full thickness of a shear-hardened steel. A very important microstructural feature that controls the energy required for crack propagation is the effective grain size, which is defined as the size of grains defined by high-angle grain boundaries (HAGB) with misorientations of 15° or higher [23]. A smaller effective grain size reduces the degree of dislocation pile-up at grain boundaries, thereby reducing local stress concentrations and inhibiting crack propagation [23,24].

However, the HE test in which the punched edge is expanded in a stretch-flanging operation, is preceded by punching the steel, which results in severe local work hardening and the formation of microstructural damage (voids) near the punched wall. The extent of this internal microstructural damage depends largely on the amount and nature of second-phase constituents and the degree of strain incompatibility or difference in micro-hardness between these second-phase constituents and the surrounding matrix [3-8]. The degree of microstructural damage or void density induced by punching will also heavily influence the ease with which a crack can propagate through the full thickness of the steel since voids will grow and coalesce during hole expansion [3-8].

In case of an essentially single-phase microstructure, the aspect of damage no longer plays a prominent role for HEC. Several studies have shown that the HEC of such single-phase steels is largely controlled by plasticity and that it has a correlation with the minimum r-value [3,9,10], which for hot-rolled steels is typically the r_0 or r_{90}. Increasing the minimum r-value, for instance by reducing the degree of planar anisotropy, is beneficial for the HEC of such steels as it postpones local necking. Such an increase of the minimum r-value and reduction of planar anisotropy can be realised via process, alloy, or both [18,25]. Reducing the degree of hot-rolling in the finishing train of the hot-strip mill below T_{nr} reduces the planar anisotropy and increases the minimum r-value [18,25], thus promoting increased HEC. This effect can be achieved by increasing the finish-rolling temperature (FRT) or by changing the type and amount of micro-alloying elements such that T_{nr} decreases or a combination of both approaches.

In this context, fracture toughness and HEC are expected to be to some extent related through similar microstructural dependencies that control the ease of crack propagation, such as grain refinement [22]. However, it also shows that both parameters can essentially differ from each other with high HEC combined with low toughness and vice versa due to different microstructural dependencies or due to differences in the extent to which both depend on common microstructural factors, such as microstructural damage through second-phase constituents and plasticity through the minimum r-value or the degree of planar anisotropy. In this Section attention will be paid to the:

I. **linear relationship** between fracture toughness and HEC
II. **discrepancy** between fracture toughness and HEC

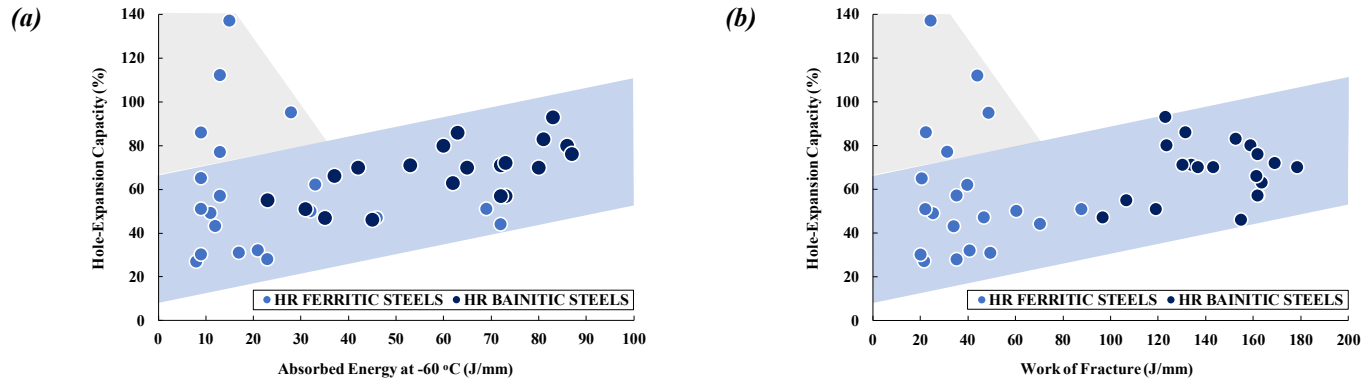

Figure 12. Hole-expansion capacity plotted against (a) the absorbed energy at -60 °C and (b) the work of fracture

I. LINEAR RELATIONSHIP BETWEEN FRACTURE TOUGHNESS AND HEC

In Figure 12, the HEC is plotted against KV_{-60} from CVN testing and WOF from DDC testing. The data show an overall weak trend (blue region) of increased impact or fracture toughness with increased HEC. This general trend, also seen for HEC versus KV_{+20} but not shown here, corroborates previous studies that HEC and toughness are correlated via a linear relationship [11,12]. This linear relationship indicates that a reduced effective grain size or a more homogeneous effective grain size distribution, which are known to yield increased toughness [18], can also help to obtain increased HEC.

The beneficial influence on toughness of grain refinement is illustrated by the data in Figure 13. Here, the WOF determined with DDC testing is plotted against the average effective grain size determined with quantitative EBSD analyses for the laboratory hot-rolled ferritic and bainitic steels. The data for both steel types is split into high and low finish rolling, i.e., FRT of 980 and 890 °C. The data plotted in Figure 13 show that the WOF and hence the fracture toughness increases with reduced effective grain size and that lowering the FRT is beneficial to promote grain refinement and increased fracture toughness.

In addition to the average grain size, the grain size distribution also plays an important role with regard to toughness. Figures 14a to 14c show the microstructures of three ferritic steels, namely F-V 980-630, F-TiV 890-580, and F-NbV 890-580, which are also highlighted in the graph shown in Figure 13. The WOF of F-V 980-630 and F-TiV 890-580 is similar with a value around 25 J/mm though the average effective grain size of the latter is considerably smaller, i.e., 4.0 versus 1.5 µm. The fact that F-TiV 890-580 with a substantially smaller average grain size has a comparably low WOF as F-V 980-630 is attributed to the grain size distribution. As Figure 14b shows, the grain structure of the F-TiV 890-580 is inhomogeneous, with coarse-grained regions surrounded by regions of much smaller grains. Only when the microstructure becomes substantially more homogeneously fine-grained, as seen for the microstructure of F-NbV 890-580 shown in Figure 14c, is the WOF substantially higher with a value of

around 88 J/mm. Also for the bainitic steels, increased homogeneity in effective grain size is expected to contribute to increased work of fracture. The data for the bainitic steels in Figure 13 seem to suggest this: lower FRT leads to increased WOF though the average effective grain size hardly changes. Based on EBSD, the increased WOF is attributed to a narrower grain size distribution.

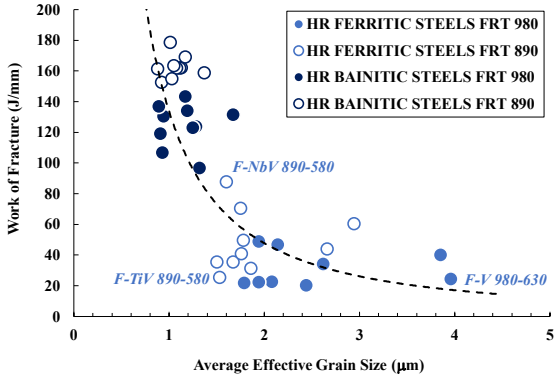

Figure 13. The work of fracture plotted against the average effective grain size

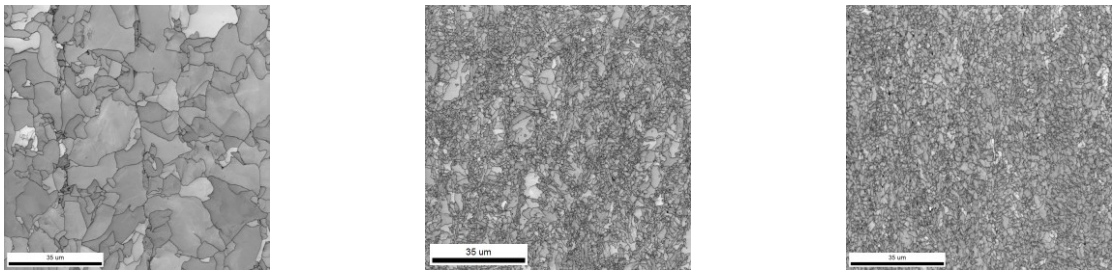

(a) F-V 980-630 *(b) F-TiV 890-580* *(c) F-NbV 890-580*

Figure 14. Image quality maps at ¼ strip thickness (100 x 100 µm, rolling direction oriented vertical)

II. DISCREPANCY BETWEEN FRACTURE TOUGHNESS AND HEC

Part of the data plotted in Figures 12a and 12b confirms the linear relationship (blue region) between toughness and HEC reported in literature [11,12]. However, the data plotted in both Figures also show that in the low-toughness domain there are steels with high HEC that deviate from this trend (grey region). This points to a discrepancy between HEC and toughness that may also exist, indicating that HEC and toughness are not entirely determined by identical parameters or not to the same extent by common microstructural and mechanical parameters. Key aspects related to this discrepancy between HEC and toughness are:

1. **microstructural damage** (void nucleation, growth, and coalesence) through second-phase constituents
2. **plasticity** through the minimum r-value and planar anisotropy.

(a) *(b)*

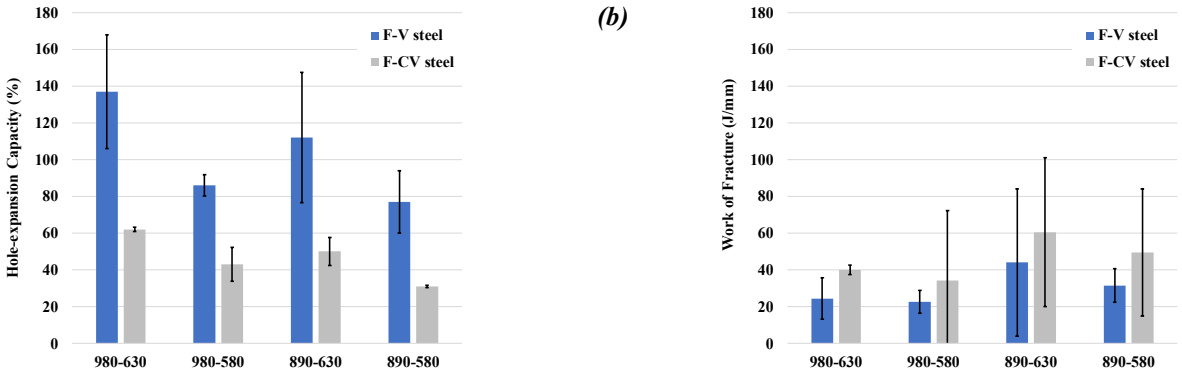

Figure 15. The (a) hole-expansion capacity and (b) work of fracture of the F-V and F-CV steels

(a) *(b)*

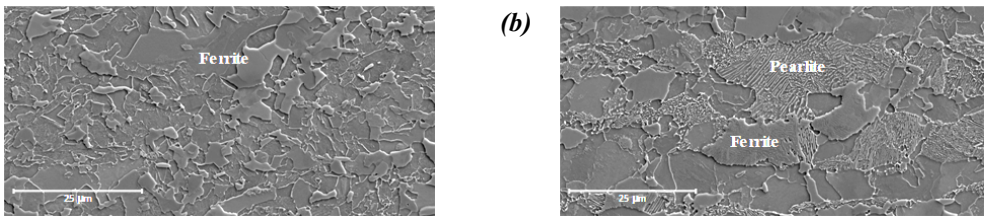

Figure 16. Microstructures (SEM) of laboratory hot-rolled (a) F-V and (b) F-CV steels with FRT and CT of 890 and 630 °C

For the ferritic steels, the relevance of microstructural damage through the presence of second-phase constituents with regard to HEC, is illustrated by Figure 15a, showing the HEC of the F-V steels with an essentially single-phase ferritic microstructure and that of the F-CV steels with ferritic microstructures with a substantial amount of coarse cementite and large pearlite colonies. To illustrate the difference in microstructures of these steels, two examples are shown in Figure 16 with microstructures of the F-V

890-630 and F-CV 890-630 steels. The data in Figure 15a show the advantage in terms of HEC of a single-phase ferritic steel over a ferritic steel with a substantial fraction of second-phase constituents. The HEC of the F-V steels is roughly twice as high as that of the F-CV steels produced with equivalent process settings. On the other hand, as illustrated by Figure 15b, the WOF or fracture toughness of these steels produced with equivalent process settings is largely comparable, taking into account the slightly lower yield strength of the F-CV steels compared to the F-V steels (Table 2). This illustrates that damage through second-phase constituents and void nucleation and growth at matrix-particle interfaces has a dramatic influence on HEC, but not necessarily on the fracture toughness, resulting in a discrepancy between HEC and toughness.

The data in Figures 15a and 15b also show that a decrease in FRT results in a decrease in HEC, while WOF or toughness increases on average. The increase in toughness can be explained by an increase in average effective grain size as discussed earlier, while the decrease in HEC is attributed to a change in plasticity through the increase of planar anisotropy and a subsequent decrease of the minimum r-value [3,9,10]. This decrease in minimum r-value promotes the early onset of local necking and promotes through-thickness crack propagation and premature failure in the HE test. This inverse relationship between the average effective grain size on the one hand and the minimum r-value through planar anisotropy on the other hand with a change in FRT and change in the degree of rolling below T_{nr} is another cause for the discrepancy between HEC and toughness as seen in Figures 12a and 12b.

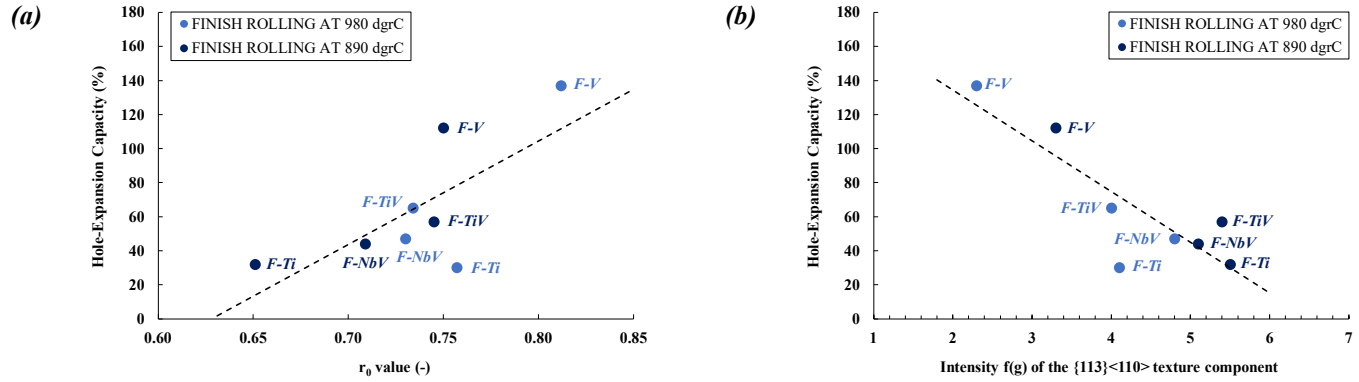

Figure 17. The hole-expansion capacity plotted against (a) the r_0-value and (b) the intensity of the {113}<110> texture component for the F-V, F-NbV, T-TiV, and F-Ti steels produced with FRT's of 980 and 890 °C and coiling at 630 °C

The degree of rolling below T_{nr} and thus the degree of planar anisotropy and the minimum r-value, is not only affected by process through the FRT [18,25] but also by the alloy composition through the choice of MA elements like V, Nb, and Ti [18,19]. Figures 17a and 17b show the HEC of the single-phase ferritic F-V, F-NbV, F-TiV, and F-Ti steels produced with FRT values of 980 and 890 °C and coiling at 630 °C plotted against the r_0-value, which is assumed here to represent the minimum r-value, and the intensity of the {113}<110> texture component. This texture component, like the neighbouring {112}<110> on the α-fibre in the ODF , is known to be related to anisotropy [26]. The data in Figure 17a corroborate previous studies that found that for single-phase ferritic steels, or for steels without a prominent role of damage on HEC, the HEC has a linear correlation with the minimum r-value: increased minimum r-value yields increased HEC. This increased minimum r-value is due to reduced planar anisotropy through increased hot-rolling above T_{nr} with micro-alloying additions that have reduced lift on T_{nr} and promote austenite recrystallisation.

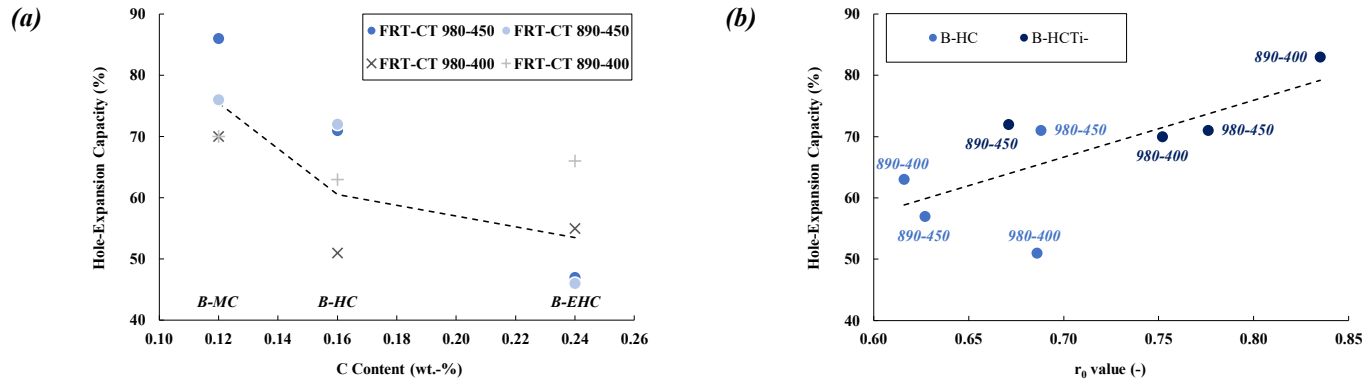

Figure 18. Hole-expansion capacity against (a) C content of B-MC, B-HC, and B-EHC and (b) r_0 of B-HC and B-HCTi-

The data in Figure 17a and 17b show the effect of the minimum r-value and texture on HEC. Figure 17a shows that the HEC of the F-V steels, in particular when produced with a high FRT, is by far higher than that of the ferritic steels with a Nb addition or V partially or fully replaced by Ti. The same effect, but now seen via texture, can be seen in Figure 17b with HEC plotted against the intensity of the {113}<110> texture component. An increase of the intensity of the {113}<110> texture component through increased planar anisotropy with increased rolling below T_{nr} results in decreased HEC.

The aspect of microstructural damage through the presence of second-phase constituents and that of planar anisotropy is also seen for the hot-rolled bainitic steels. Figure 18a shows HEC plotted against C content of the B-MC, B-HC, and B-EHC steels. The data show that increased C content and subsequently increased second-phase fraction reduces HEC. Figure 18b with HEC plotted against r_0 for the B-HC and B-HCTi- steels illustrates the effect of the minimum r-value through planar anisotropy and Ti content. The data show that the B-HCTi- steels with a reduced Ti content and hence with slightly lower T_{nr}, favouring increased austenite recrystallisation during finish rolling and decreased planar anisotropy, generally have a higher r_0-value and a higher HEC than the B-HC steels with increased Ti. The effect of r_0 on HEC seen in Figure 18b for the bainitic steels is much less than that

observed earlier for the ferritic steels in Figure 17a. This can be explained by the fact that for the bainitic steels the aspect of plastic anisotropy is likely overshadowed by that of microstructural damage through an increased fraction of second-rich phase constituents.

The complex relationship between HEC and fracture toughness seen in this study shows that both parameters can be dominated by different microstructural dependencies or by common microstructural dependencies, but to different degrees. Fracture toughness is largely determined by average effective grain size (distribution), while HEC is largely determined by the presence of second-phase constituents through damage and void formation upon shearing and by texture through planar anisotropy and minimum r-value through postponed local necking during stretch-flanging. All of these microstructural features that control fracture toughness and HEC are ultimately controlled by alloy composition and process. Optimal HEC is achieved by minimising the amount of second-phase constituents and – in case of a multi-phase microstructure – by reducing strain incompatibilities between matrix and second-phase constituents through transformation strengthening, temper softening, or precipitation strengthening. Another approach is to minimise the planar anisotropy and to increase the minimum r-value through reduced deformation below T_{nr}, either via increased FRT in the hot-strip mill or via suitable micro-alloying. However, this comes at the expense of fracture toughness, as this approach typically results in a larger effective grain size of the final microstructure if no countermeasures are taken. Although such countermeasures can pose a technological challenge in the hot-strip mill, only by achieving a homogeneous, fine-grained, and isotropic microstructure with little or no second phase will an optimum balance between HEC and fracture toughness be achieved.

2G. Discussion – Fracture Toughness and Hole-Expansion Capacity of Industrial Steels

Both the HE and DDC test provide information on edge-crack sensitivity, albeit under different conditions. In case of the HE test, an essentially single stress-strain path is imposed via stretch-flanging with the shear-hardened edge under tensile stress. In contrast, in the initial stage of the DDC test highly compressive stresses are imposed followed by tensile stresses due to springback. This alternating stress state in the DDC test can cause significant secondary cold work embrittlement, depending on the type of steel being examined. As such, the HE and DDC tests provide essentially different measures of edge ductility as was already confirmed by the results discussed in Section 2F. Results obtained for industrial steels with both tests described in this Section confirm this.

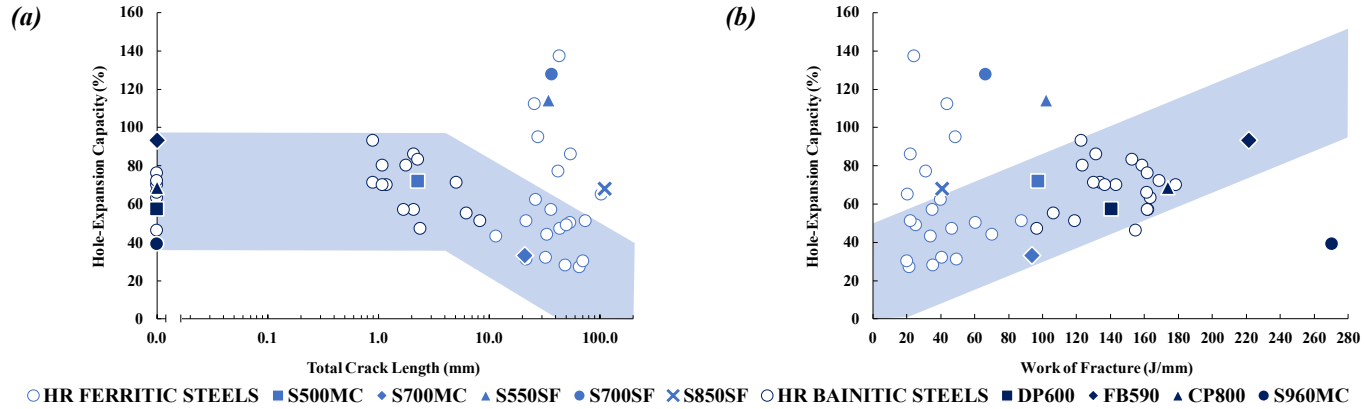

Figure 19. The hole-expansion capacity plotted against (a) the total crack length and (b) the work of fracture

In Figure 19a the HEC of the laboratory hot-rolled ferritic and bainitic steels are plotted against the TCL values from DDC testing and supplemented with comparable data for a number of hot-rolled industrial steels from regular production and works trials, which also appeared in Section 2E. The data show the relevance of DDC next to HE testing to assess crack susceptibility. Steels with high HEC can be free of cracks after deep drawing in the DDC test, but can also be highly crack susceptible through increased secondary cold work embrittlement and reduced fracture toughness during the initial stage of the DDC test. On the other hand, steels with only a limited HEC, can still do very well in the DDC test with crack-free samples after initial deep-drawing. A good example of this is the martensitic S960MC with a relatively low HEC of circa 40% but with no cracks after cup deep drawing. However, a ferritic S700MC with similar HEC as the S960MC performs much poorer in the cup deep-drawing stage of the DDC test with an abundance of small cracks in compressed regions of deep-drawn cups and thus a substantially higher TCL value.

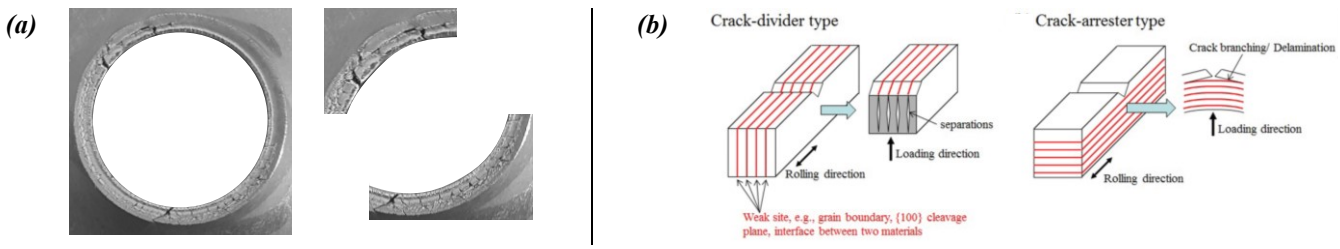

Figure 20. (a) HE sample of a delaminated HSLA and (b) delamination as crack divider and crack arrester [27]

The data in Figure 19b shows HEC values of the laboratory hot-rolled ferritic and bainitic steels plotted against the WOF from DDC testing and supplemented with comparable data for hot-rolled industrial steels from hot-strip mill production and works trials. Part of the data from the industrial steels corresponds well with the linear relationship between HEC and toughness. However, part of the industrial data reiterates the discrepancy between HEC and toughness with several high stretch-flangeable HSLA steels (SF) with high HEC and low fracture toughness. The high HEC of these essentially single-phase ferritic steels is again associated – at least in part – with a high minimum r-value due to low planar anisotropy via high finish rolling. At the same time this high finish rolling leads to a coarse-grained microstructure and low fracture toughness. Apart from this discrepancy between HEC and

toughness in the low-toughness domain, there also appears to be a discrepancy in the high-toughness domain with the martensitic S960MC steel. This steel has a high WOF due to a small effective grain size, but has a low HEC, which is attributed to a low minimum r-value through high planar anisotropy due to low finish rolling to promote grain refinement and high toughness.

Close inspection of HE test samples for some steels also suggests another aspect that can contribute to an unfavourable mix of high HEC and low fracture toughness. The propagation of through-thickness cracks in HE test samples during stretch-flanging may be deflected or arrested by the presence of delaminated planes in the RD-TD plane parallel to the sheet surface, which postpones failure in the HE test. An example of this is given by Figure 20a with the stretch-flanged edge of a HE test sample of an industrial hot-rolled ferritic HSLA steel. These delaminated planes, which result from shearing prior to HE testing or during the stretch-flanging operation of the HE test itself, are RD-TD planes that are weakened through certain microstructural irregularities, such as chemical segregation, particles, elongated grains, and the presence of {100} cleavage planes [27]. These weak planes are susceptible to delamination via cleavage fracture and, depending on their orientation relative to mechanical loading, can act as a crack divider or as a crack arrester (Figure 20b) [27,28]. In case of the HE test, the through-thickness cack travelling from the burr progresses perpendicular to the weak planes and hence the crack-arrester functionality of the RD-TD weak planes can be activated.

3. SAE J2334 Corrosion Resistance – The Role of Alloying Elements for Hardenability

In the previous Sections, it was shown that bainitic CP steels provide superior toughness over ferritic HSLA steels without sacrificing edge ductility based on the HE test. These CP steels with a small effective grain size are obtained with suitable rolling and cooling in the hot-strip mill and the use of specific alloying elements for sufficient hardenability to obtain a bainitic microstructure. Common alloying elements to gain hardenability are Mn, Cr, and Mo. However, these elements also affect the steel's corrosion resistance. A beneficial effect of these elements is expected, especially for Cr, which is generally known to reduce corrosion rates [29], but it is known that the effect is highly dependent on specific details of the corrosive conditions and that the effect of alloying elements can vary [30]. The role of alloying elements on the steel's corrosion resistance is important because it ultimately affects the integrity and lifetime of exposed automotive components, such as chassis and frame applications.

Here, the influence of Mn, Cr, and Mo on the SAE J2334 corrosion resistance [31] is investigated for a number of laboratory hot-rolled HR660Y760T-CP steels. The alloys with various combinations of Mn, Cr, and Mo were designed to provide similar tensile properties through comparable hardenability based on the critical metal parameter (Pcm).

Table 4. Compositions (in wt-%) and the hardenability coefficient Pcm

Alloy	C	Mn	Si	Al	Ti	Cr	Mo	N	Pcm
120Mn95Cr		1.20				0.95	-		0.21
160Mn55Cr		1.60				0.55	-		0.21
190Mn25Cr		1.90				0.25	-		0.21
215Mn00Cr	0.093	2.15	0.17	0.03	0.105	-	-	0.004	0.21
120Mn55Cr10Mo		1.20				0.55	0.10		0.19
120Mn35Cr20Mo		1.20				0.35	0.20		0.19
120Mn00Cr30Mo		1.20				-	0.30		0.18

Table 5. Tensile properties (L) of the HR660Y760T-CP steels

Steel	Rp (MPa)	Rm (MPa)	A50 (%)
120Mn95Cr	758	852	16.5
160Mn55Cr	740	829	15.8
190Mn25Cr	747	825	14.6
215Mn00Cr	726	797	11.9
120Mn55Cr10Mo	716	800	14.0
120Mn35Cr20Mo	723	799	15.0
120Mn00Cr30Mo	770	832	14.6

The compositions and Pcm coefficients are given in Table 4. The P and S contents were circa 0.01 wt-% and 10 ppm. The alloys were melted in a vacuum-induction furnace and ingot cast. The ingots were forged from 105 to 35 mm thickness after 1240 °C reheating and left to cool to ambient temperature before being sawn in smaller blocks of 75 x 105 mm. These blocks were rolled in a 4-pass rolling schedule to 3.5 mm in a single-stand mill after reheating to 1240 °C for 40 minutes. The FRT was 950 °C. After hot rolling, the plates, measuring 750 x 105 x 3.5 mm, were directly transferred to a run-out-table (ROT) and cooled with a mixture of water and pressurized air with a cooling rate of roughly of 50 °C/s before being placed in a furnace to replicate coil cooling. The exit ROT and furnace temperature was 540 °C. All plates were shot-blasted to remove oxides from the hot-rolling process prior to sampling for mechanical and corrosion testing. The tensile properties in longitudinal direction (L) are shown in Table 5.

The corrosion resistance was determined with the SAE J2334 test. This field-correlated test for automotive coatings was developed in the late 1980s in the US to replicate the degradation mechanisms that occur in real-life situations and provide the best correlation with regard to cosmetic performance observed in field tests with vehicles [17]. The SAE J2334 protocol uses a solution of 0.5% NaCl, 0.1% $CaCl_2$ and 0.075% $NaHCO_3$ with a pH of 7 ± 0.5. The tests were caried out in a Q-FOG Controlled Relative Humidity (CRH) Cyclic Corrosion Tester (model CRH1100). The test consists of three stages: (1) a humid stage with a relative humidity (RH) of 100% for 6 hours at 50 °C, (2) a salt application stage for 15 minutes at ambient conditions, and (3) a dry stage with a RH of 50% for 17 hours and 45 minutes at 60 °C (or in the weekend a duration of 48 hours). The mass loss (ML) was evaluated after 37, 60 and 90 days. Here, only the ML-90 data is reported. The samples measured 25.4 x 50.1 x 3.2 mm with in the

centre a punched hole with a 39.3 mm diameter for fixture to the sample holder with a synthetic screw. The mass loss was determined by removing the corroded product by shot peening and measuring the weight reduction in mg/mm^2.

Comparative measurements were executed using VDA 233-102 and VDA 621-415 tests for 10 weeks (70 days). It was found that the periods at high humidity and high temperature during daily cycles in the SAE J2334 test play a key role in differences in the measured mass loss rate for different alloys compared to those measured in the VDA 233-102 and VDA 621-415 tests, operating at significantly lower temperatures in daily and weekly cycles. The SAE J2334 test has longer periods of enhanced corrosivity compared to the VDA tests and therefore different conditions for precipitation and patina formation. This alters the effect of alloying elements on corrosion, as different oxides and structures occur.

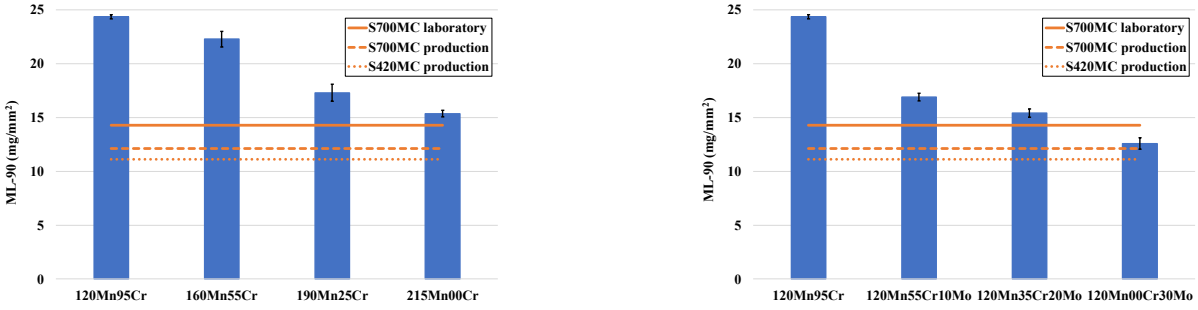

(a) varying Cr and Mn contents *(b) varying Cr and Mo contents*

Figure 21. Mass loss after 90 cycles (ML-90) in the SAE J2334 test for the laboratory HR660Y760T-CP steels.

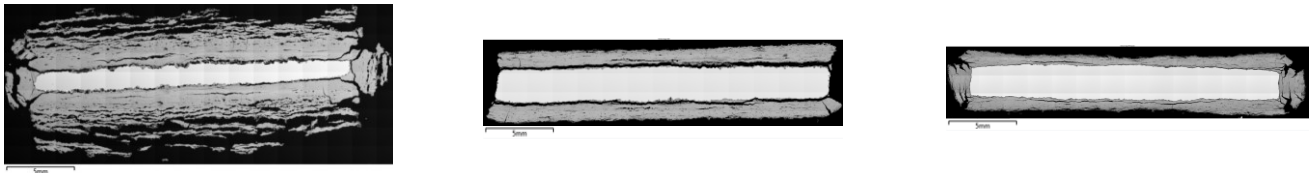

(a) 120Mn95Cr *(b) 215Mn00Cr* *(c) 120Mn00Cr30Mo*

Figure 22. SEM-BS images of the corroded samples and corrosion products after 90 cycles of the SAE J2334 corrosion test

The ML-90 data are shown in Figure 21. Figure 21a shows the ML-90 data for the range of HR660Y760T-CP steels with various Cr and Mn contents. Similar data for the range of HR660Y760T-CP steels with various Cr and Mo contents are shown in Figure 21b. The data in both Figures show that reducing the Cr content and replacing it with Mn or Mo to maintain a similar degree of hardenability leads to a substantial decrease in ML-90 and thus to a significant increase in corrosion resistance based on the SAE J2334 test. Figure 22 shows SEM Backscatter (BS) images of the cross sections of the 120Mn95Cr, 215Mn00Cr and 120Mn00Cr30Mo steels and confirms the dramatic influence of Cr on the corrosion rate. The 120Mn95Cr steel shows pronounced exfoliation (dark grey areas in SEM-BS), which is absent for the 215Mn00Cr and 120Mn00Cr30Mo steels.

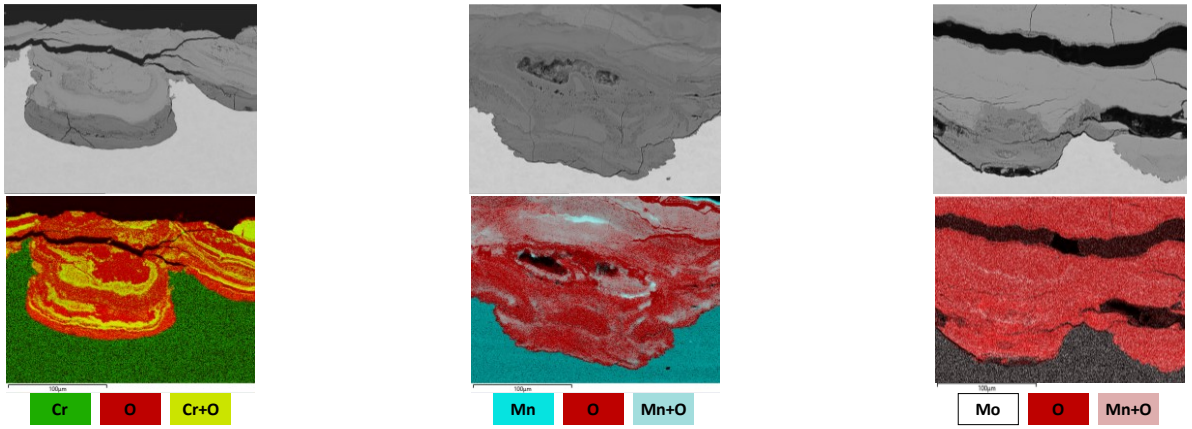

(a) 120Mn95Cr *(b) 215Mn00Cr* *(c) 120Mn00Cr30Mo*

Figure 23. SEM-BS images and SEM-EDX mappings of corrosion pits after 90 cycles SAE J2334

The adverse influence of Cr on the SAE J2334 corrosion rate is believed to be caused by three consecutive steps in the corrosion process. The first step occurs in shallow pits at the steel-corrosion interface, where the steel dissolves in the presence of an enhanced Cl concentration. In this solution, chromium oxide precipitates prior to iron oxide [32], and forms lamellae. This is illustrated by Figure 23a for the 120Mn95Cr steel, showing evidence of distinct lamellae rich of chromium oxides in the corrosion pits. Although not shown, such lamellae are already seen with as little as 0.25 wt-% Cr (190Mn25Cr). Such pronounced lamellar structures are absent in the corrosion pits of the Cr-free 215Mn00Cr and 120Mn00Cr30Mo steels as shown by Figures 23b and 23c. This indicates that Mn and Mo, at least at the levels present in these alloys, do not yield a similar corrosion response as Cr.

The formation of lamellae rich in chromium oxides in the corrosion pits at the steel-corrosion interface results in the second step, which is the accumulation of chromium-oxide rich lamellae in the corrosion product. This leads to alternatingly layers of enriched chromium oxide and pure iron oxide. An example of this for the high-Cr 120Mn95Cr steel is shown in Figure 24a.

The third and final step is the formation of voids immediately next to the chromium-enriched agglomerates (see detailed image overlay of Figure 24a), which disrupts the regular formation of a compact oxide layer or patina. These voids fill with chloride-rich water during each wetting stage of the test cycle, leaving an open structure, which becomes partially filled with soluble iron oxychlorides during the drying stage. This repeated process leads to lateral growth of the voids until they coalesce and form channels throughout the oxide layer. As a consequence, a layered structure of alternating dense layers of chromium oxide and open layers of iron oxide begins to build up into a highly porous structure to the point where exfoliation occurs. Figure 24a showing an SEM-BS image and a Cr elemental SEM-EDX mapping of the exfoliating corrosion product of the high-Cr 120Mn95Cr steel confirms this. Such an exfoliated structure is absent for the Cr-free 215Mn00Cr and 120Mn00Cr30Mo steels as illustrated by Figures 24b and 24c. Both the horizontal channels due to void coalescence and the vertical channels due to decohesion and exfoliation leave passageways for enhanced ion mobility to and from the steel surface. This promotes further corrosion for Cr-rich steels in the SAE J2334 test.

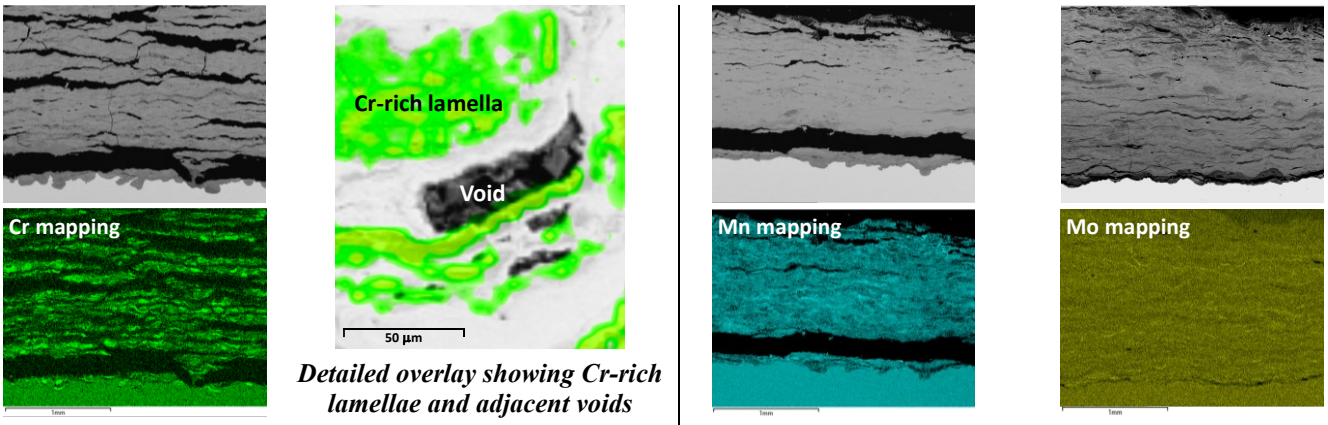

Detailed overlay showing Cr-rich lamellae and adjacent voids

(a) 120Mn95Cr *(b) 215Mn00Cr* *(c) 120Mn00Cr30Mo*

Figure 24. SEM-BS images and SEM-EDX mappings of the corrosion product after 90 cycles SAE J2334

The outcome of the SAE J2334 test is in stark contrast with that from the two comparative VDA tests, which do not show a significantly increased corrosion rate for Cr-rich steels. Although Cr-rich lamellae and agglomerates are also formed in corrosion deposits in the VDA tests, the step of void formation leading to a porous patina, does not occur. Instead, a compact patina is formed that is not prone to exfoliation, resulting in nearly identical mass loss for all HR-660Y760T-CP steels irrespective of composition.

The ML-90 data were fitted with a linear equation based on the contents of Cr, Mn, and Mo in wt-% and at-%, yielding the following two empirical equations for ML-90 expressed in mg/mm^2:

$$ML - 90 = 17.2\%Cr + 7.2\%Mn + 8.8\%Mo \quad (R^2 = 0.92) \quad \text{with Cr, Mn, and Mo in wt-\%} \quad [5]$$

$$ML - 90 = 16.1\%Cr + 7.1\%Mn + 15.0\%Mo \quad (R^2 = 0.92) \quad \text{with Cr, Mn, and Mo in at-\%} \quad [6]$$

Equation [5] with contents in wt-% shows that at the alloy levels used here, which are considered typical for HR660Y760T-CP, Cr stands out in its detrimental effect on SAE J2334 corrosion resistance, while Mn and Mo at the levels used here show a much less harmful effect. For Mn this can be understood as manganese oxide precipitates simultaneously with iron oxide and therefore spreads evenly through the patina. This promotes a homogeneous and less porous corrosion product, which does not impair the protective effect of the patina. This explains the minimal ML-90 increase seen in Figure 21a for 215Mn00Cr compared to the S700MC laboratory reference and the fact that Mn has a small effect on ML-90 in both Equations and therefore on corrosion rate.

Equation [6] with contents in at-% shows that Mo behaves similar to Cr. This can be understood by considering the solubility of molybdenum oxide, which, like chromium oxide, is significantly lower than that of iron oxide. This results in the formation of lamellae, which are indeed observed in the Mo elemental mapping in pits at the corrosion-steel interface (Figure 23c) and throughout the corrosion product (Figure 24c). As with Cr, these lamellae disrupt the formation of adjacent compact oxide, thus creating voids that in turn lead to a higher corrosion rate. The much weaker lamellar formation for 120Mn00Cr30Mo (Figure 23c) than for 120Mn95Cr (Figure 23a) is attributed to the lower Mo content that is needed to obtain the same hardenability effect [33].

4. Leveraging Fracture Toughness and Corrosion Resistance in the Development of MP800

The knowledge gained from the study of fracture toughness and corrosion resistance has been leveraged in the development of a new HR660Y760T-CP grade (Table 6) for automotive chassis and frame applications, i.e., MP800. Instead of the conventional focus on stretch-flangeability and HEC, the approach was widened to include also fracture toughness through DDC testing to assess crack susceptibility under conditions that take into account secondary cold work embrittlement and replicate component manufacturing through successive forming operations with alternating compressive and tensile stresses. Additionally, SAE J2334 corrosion resistance was incorporated into the design of the new bainitic MP800 by adopting a Cr-free approach (Table 7) to achieve SAE J2334 corrosion resistance equivalent or better than that of HSLA of equivalent strength (S700MC) and by using a CMn alloy to achieve sufficient hardenability for optimal mechanical properties in a cost-effective and therefore Mo-free approach.

Table 6. VDA norm for HR660Y760T-CP and typical mechanical properties of MP800

	Test direction	Yield strength $R_{p0.2}$ (MPa)	Tensile strength R_m (MPa)	A80 (t ≤ 3mm) (%)	A50 (t > 3mm) (%)	HEC (%)
VDA norm (239-100)	L	660 – 820	760 – 920	≥10	≥11	≥50
Typical	L	700	800	13	14	50 – 80

Table 7. Composition MP800 (in wt-%)

C	Mn	Si	Al	P	S	Nb+Ti	Cr	Mo	N
<0.1	<2.0	<0.5	0.02 – 0.06	<0.015	<0.002	<0.15	<0.01	<0.01	<0.0060

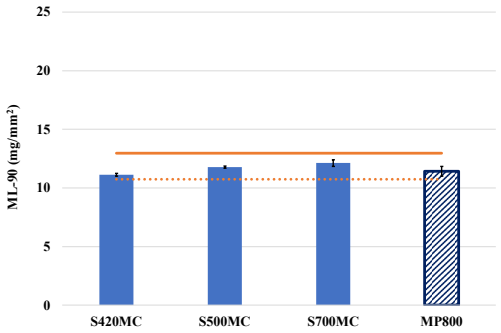

Figure 25. Mass loss after 90 cycles (ML-90) SAE J2334 corrosion testing (lines cover the typical HSLA domain)

Figure 25 shows ML-90 data from SAE J2334 corrosion testing of a number of hot-rolled conventional HSLA grades and the new MP800. The data show that the SAE J2334 corrosion resistance of the MP800 is within the range covered by conventional HSLA grades and that MP800 performs similarly or slightly better than S700MC with equivalent tensile strength.

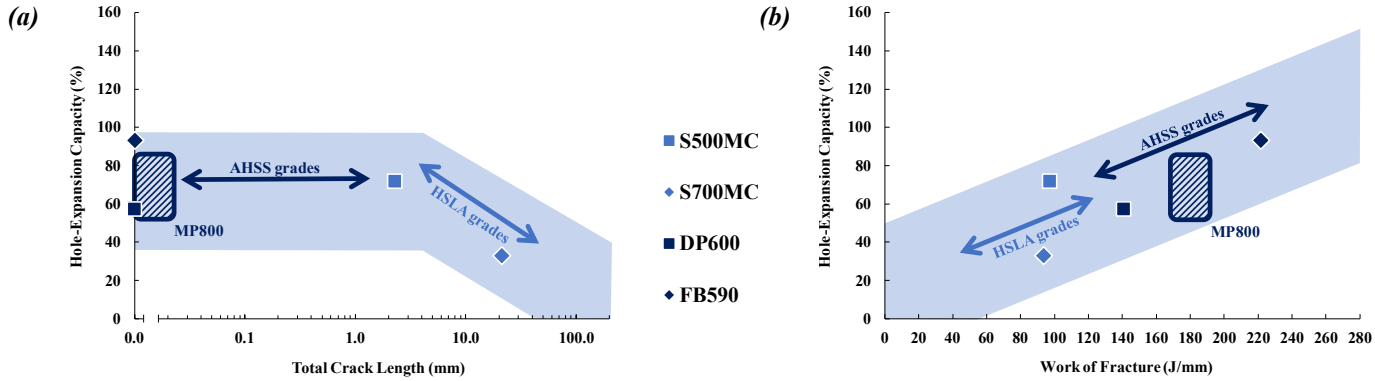

Figure 26. The hole-expansion capacity plotted against (a) the total crack length and (b) the work of fracture

The main benefit of the new MP800 over S700MC is its improved balance of high HEC combined with high fracture toughness and low (edge) crack susceptibility due to secondary cold work embrittlement. Figure 26 shows the benefit of the new bainitic MP800 grade. In addition to offering high yield and tensile strength to reduce component weight for automotive applications via down-gauging, the new bainitic MP800 combines high HEC for demanding component geometries with an adequate level of fracture toughness and high edge-crack resistance that promises trouble-free component manufacturing. This excellent combination of stretch-flangeability and fracture toughness with SAE J2334 corrosion resistance comparable to conventional HSLA grades with equivalent strength, makes the new bainitic MP800 suitable for demanding light-weight automotive chassis and frame applications.

5. Conclusions

Two main aspects were investigated for hot-rolled steels used in automotive chassis and frame applications. The first aspect concerns the susceptibility to secondary cold work embrittlement and the fracture toughness of ferritic HSLA and bainitic CP steels as determined in a deep-draw cup (DDC) test and how fracture toughness and HEC relate to each other through different microstructural dependencies. The second aspect concerns the SAE J2334 corrosion resistance of HR660Y760T-CP steels and the effect of the alloying elements Mn, Cr, and Mo used for optimal hardenability of these bainitic steels. The knowledge gained from these two investigations was leveraged in the development of a new HR660Y760T-CP grade. The conclusions are as follows:

- The DDC test is an effective method to screen steels on edge-crack susceptibility due to secondary cold work embrittlement and fracture toughness and provides an essential addition to HE testing as it replicates better the effect of alternating stresses on edges during successive forming operations and intermediate springback in press shops.
- Results from DDC and HE tests on hot-rolled high-strength ferritic HSLA and bainitic CP steels demonstrate that CP steel provide a superior balance between HEC and fracture toughness compared to HSLA steel.
- Results from DDC and HE tests on hot-rolled high-strength ferritic HSLA and bainitic CP steels reveal a complex relationship between HEC and fracture toughness with partly a linear relationship between both parameters, but also a discrepancy for steels with high HEC and yet low fracture toughness.
- The complex relationship between HEC and fracture toughness shows that both parameters can be dominated by different microstructural features or by common microstructural dependencies, but to different degrees. Fracture toughness is largely controlled by average effective grain size and distribution, while HEC is (also) largely controlled by the presence of second-phase constituents through void formation upon shearing and by texture through planar anisotropy, r-value and postponed local necking during stretch-flanging. All these microstructural features are ultimately controlled by alloy and process.
- Optimum HEC is achieved by minimising the amount of second phase or by reducing strain incompatibilities between matrix and second phase. Another approach would be to minimise the planar anisotropy and raise the minimum r-value

through reduced deformation below T_{nr}, either via increased FRT or suitable micro-alloying. However, this comes at the expense of fracture toughness, as this results in a larger effective grain size if no countermeasures are taken. Although such countermeasures can pose technological challenges in the mill, only by achieving a homogeneous, fine-grained, isotropic microstructure with little or no second phase will an optimum balance between HEC and fracture toughness be achieved.

- SAE J2334 corrosion testing on HR660Y760T-CP steels with various Mn, Cr, and Mo contents shows that Cr has a detrimental effect on the corrosion rate due to the formation of Cr-rich lamellae and agglomerates, promoting a porous patina that leads to accelerated corrosion of the steel substrate. This accelerated corrosion is not seen for Cr-free CP steels that rely for hardenability exclusively on Mn or a combination of Mn and Mo.
- Knowledge on the relationship between HEC and fracture toughness and that of the role of Mn, Cr, and Mo on corrosion resistance has been leveraged in the development of a new Cr-free HR660Y760T-CP grade for automotive chassis and frame applications. This new MP800 promises to deliver an excellent combination of stretch-flangeability and fracture toughness with SAE J2334 corrosion resistance comparable to conventional HSLA grades with equivalent strength.

References

1. A. Rijkenberg et al., “Stretching Strength and Formability for Increased Performance and Mass-savings in Automotive Chassis Applications”, Steels in Cars and Trucks 2017, Noordwijk, The Netherlands, 2017.
2. K. Seto, Y. Funakawa, S. Kaneko, “Hot Rolled High Strength Steels for Suspension and Chassis Parts “NANOHITEN” and “BHT” Steel”, JFE Tech. Report, No. 10, 2007.
3. S.K. Paul, “A Critical Review on Hole Expansion Ratio”, Materialia, Vol. 9 (100566), 2020, and references therein.
4. K. Hasegawa, K. Kawamura, T. Urabe, Y. Hosoya, “Effects of Microstructure on Stretch-Flange Formability of 980 MPa Grade Cold-Rolled Ultra High Strength Steel Sheets”, ISIJ Int., Vol. 44, 2004, pp. 603-609.
5. O. Terrazas, K.O. Findley, C.J. Van Tyne, “Influence of Martensite Morphology on Sheared-Edge Formability of Dual-Phase Steels”, ISIJ Int., Vol. 57, 2017, pp. 937-944.
6. M.D. Taylor, K.S. Choi, X. Sun, D.K. Matlock, C.E. Packard, L. Xu, F. Barlat, “Correlations between Nanoindentation Hardness and Macroscopic Mechanical Properties in DP980 Steels”, Mater. Sci. Eng. A, Vol. 597, 2014, pp. 431-439.
7. Y. Takahashi, O. Kawano, Y. Tanaka, and M. Ohara. “Fracture Mechanical Study on Edge Flangeability of High Tensile-Strength Steel Sheets”, MS&T 2009: Proceedings from the Materials Science & Technology Conference, Pittsburgh, PA, USA, 2009, pp. 1317-1328.
8. M. Sudo, S.I. Hashimoto, S. Kambe, “Niobium Bearing Ferrite-Bainite High Strength Hot-Rolled Sheet Steel with Improved Formability”, Trans. ISIJ, Vol. 23, 1983, pp. 303-311.
9. A. Phillips, H. Kaul, J. Burg, C. Killmore, J. Williams, P. Campbell, W. Blejde, “Effect of Microstructure and Texture on the Edge Formability of Light Gauge Strip Steel”, ISIJ Int., Vol. 51, 2011, pp. 832-842.
10. H. Asano, N. Matsuzu, A. Itami, K. Koyama, “Development of High Strength Steel Sheet with Excellent Stretch Flange Formability for Automobile Application”, SAE Technical Paper, 940943, 1994.
11. D. Frómeta, M. Tedesco, J. Calvo, A. Lara, S. Molas, D. Casellas, “Assessing Edge Cracking Resistance in AHSS Automotive Parts by the Essential Work of Fracture Methodology”, J. Phys,: Conf. Ser. 896, 012102, 2017.
12. J.I. Yoon, J. Jung, S. Joo, T.J. Song, K. Chin, M.H. Seo, S. Kim, S. Lee, H.S. Kim, “Correlation between Fracture Toughness and Stretch-Flangeability of Advanced High Strength Steels”, Mater. Lett., Vol. 180, 2016, pp. 322-326.
13. D. Li, G. Heßling, W. Bleck, “The Secondary Work Embrittlement in Sheet Steels”, Steel Res. Int., Vol. 70, Issue 4-5, 1999, pp. 154-161.
14. A. Rijkenberg et al., “The Relationship between Hole-Expansion Capacity and Fracture Toughness Ferritic and Bainitic High-Strength Hot-Rolled Steels”, 3rd International Symposium on the Recent Developments in Plate Steels, Vail, Colorado (USA), 2-5 June 2024.
15. S. Cao, J. Zhang, J. Wu, J. Chen, “Effects of GBCD on Cold Work Embrittlement of High Strength Interstitial Free Steels”, Materials and Design, Vl. 27, 2006, pp. 53-57.
16. E. Yasuhara, K. Sakata, T. Kato, O. Hashimoto, “Effect of Boron on the Resistance to Secondary Working Embrittlement in Extra-Low-C Cold-Rolled Steel Sheet”, ISIJ Int., Vol. 34, No. 1, 1994, pp. 99-170.
17. F.W. Lutze, K.A. Smith, R. Mason, D. Nymberg, L.S. Thompson, C. Meade, L. McQuiston, Ra. Singleton, C. Handsy, SAE Transactions Vol. 112, Section 6: Journal of passenger cars - Mechanical Systems, 2003, pp. 1209-1214.
18. D.T. Llewellyn, R.C. Hudd, “Low-carbon Structural Steels”, Steels: Metallurgy and Application, 3rd Ed., Oxford, UK, Butterworth-Heinemann, 1998, pp. 137-198.
19. R. Barbosa, F. Boratto, S. Yue, J. Jonas, “The Influence of Chemical Composition on the Recrystallisation Behaviour of Microalloyed Steels”. Microstructure and Properties of HSLA Steels, The Minerals, Metals & Materials Society (TMS), Warrendale, PA, USA, 1988, pp. 51–61.
20. Tata Steel IJmuiden B.V., “Hot-Rolled High-Strength Steel Strip”, WO2024/032949A1, 15 February 2024.
21. W. Oldfield, “Curve Fitting Impact Test Data: A Statistical Procedure”, ASTM Stand. News, Vol. 3, 1975, pp. 24–29.
22. A.A. Griffith, “VI. The Phenomena of Rupture and Flow in Solids”, Philosophical transactions of the royal society of London, Series A, containing papers of a mathematical or physical character, 221 (582-593), 1921, pp. 163-198.
23. A.-F. Gourgues H.M. Flower, T.C. Lindley, “Electron Backscattering Diffraction Study of Acicular Ferrite, Bainite, and Martensite Steel Microstructures”, Materials Science and Technology, Vol. 16, 2000, pp. 26-40.
24. J. Wu, G. Bai, L. Zhao, Z. Zhang, Y. Peng, J. Chu, Q. Wang, “Effects of Finish Rolling Temperature on the Critical Crack Tip Opening Displacement (CTOD) of Typical 500 MPa Grade Weathering Steel”, Metals, Vol. 13 (10), 1791, 2023.
25. C. Capdevila, I. Toda, F.G. Caballero, C. Garcia-Mateo, C. Garcia de Andres, “Determination of Hot- and Cold-Rolling Texture of Steels: A Combined Bayesian Neural Network Model”, Materials Science and Technology, Vol 28, No. 3, 2012, pp. 321-333.
26. R.K. Ray, J.J. Jonas, “Transformation Textures in Steels”, Int. Mat. Rev., Vol. 35, 1, 1990, pp. 1-36.
27. T. Inoue, Y. Kimura, “Effect of Delamination and Grain Refinement on Fracture Energy of Ultrafine-Grained Steel Determined Using an Instrumented Charpy Impact Test”, Materials 2022, 15, 867.
28. B. Mintz, E. Maina, and W.B. Morrison, “Origin of fissures on fracture surfaces of impact samples of HSLA steels with ferrite/pearlite microstructures”, Materials Science and Technology, Vol. 23, No. 3, 2007, pp. 347-354.
29. ASTM G 101 – 97, Standard Guide for Estimating the Atmospheric Corrosion Resistance of Low Alloy Steels.
30. T. Moroishi, J. Satake, Iron and Steel (Jp) 59-2, 1973, pp. 293-300.
31. SAE Laboratory Cyclic Corrosion Test (STABILIZED Apr 2016) J2334_201604.
32. S. Dickinson, M. Bachet, R. Eaker, J. Henshaw, D. Hussey, C. Marks, P. Tremain, Proceedings Nuclear Plant Chemistry Conf. 2012, Paris.
33. M. Deepa, G. Sahoo, S.K. Dhua, “Effect of Molydenum Addition on Hardenability of Chromium-Boron Steels used for Press Hardening Applications”, J. Min. Metall. Sect. B-Metall. 54 (3) B, 2018, pp. 339 – 347.